WATER RESOURCES RESEARCH, VOL. 28, NO. 2, PAGES 411–425, FEBRUARY 1992

Friction Angle Measurements on a Naturally Formed Gravel Streambed: Implications for Critical Boundary Shear Stress

JOHN M. BUFFINGTON[1]

Forestry Sciences Laboratory, U.S. Forest Service, Juneau, Alaska

WILLIAM E. DIETRICH AND JAMES W. KIRCHNER

Department of Geology and Geophysics, University of California, Berkeley

We report the first measurements of friction angles for a naturally formed gravel streambed. For a given test grain size placed on a bed surface, friction angles varied from 10° to over 100°; friction angle distributions can be expressed as a function of test grain size, median bed grain size, and bed sorting parameter. Friction angles decrease with increasing grain size relative to the median bed grain size, and are a systematic function of sorting, with lower friction angles associated with poorer sorting. The probability distributions of critical shear stress for different grain sizes on a given bed surface, as calculated from our friction angle data, show a common origin, but otherwise diverge with larger grains having narrower and lower ranges of critical shear stresses. The potential mobility of a grain, as defined by its probability distribution of critical shear stress, may be overestimated for larger grains in this analysis, because our calculations do not take into account the effects of grain burial and altered near-bed flow fields.

INTRODUCTION

In a recent study, *Kirchner et al.* [1990] examined the problem of critical boundary shear stress in heterogeneous mixtures of sand and gravel by measuring friction angles and relative protrusion of grains on bed surfaces formed during bed load transport in a small flume. Using these measurements in the theory proposed by *Wiberg and Smith* [1987] for critical shear stress of individual grains resting in pockets of known geometry, they showed that critical boundary shear stress for a grain of a specified size is characterized by a probability distribution rather than by a single value. For a given bed surface, grains of widely different sizes were found to have approximately the same minimum critical boundary shear stress, a result consistent with aspects of the "equal mobility" hypothesis proposed by *Parker and Klingeman* [1982]. However, the distribution functions of critical shear stress diverged widely from this minimum value, such that grains much larger than the median showed a relatively narrow range of low critical shear stress, whereas the smallest grains examined spanned a broad range of critical shear stress. This indicates that a large fraction of the smallest grains would not be entrained, presumably because they reside in deep pockets between grains. The measurements and calculations of *Kirchner et al.* [1990] suggested the following hypotheses: (1) transient shear stress excursions, rather than mean shear stress, may control initial motion of the most easily entrained grains; (2) the large difference in critical shear stresses for large and small grains above a common minimum value should give rise to significant grain interactions and mobility interdependencies that in turn control surface textures and transport rates by size class; and (3) the well-known rapid rise in bed load transport rate with increasing boundary shear stress in coarse sediment is a direct consequence of the probability distribution of grain friction angles and, in turn, critical boundary shear stress.

As *Kirchner et al.* [1990] point out, their empirical relationships among friction angle, grain protrusion, and grain size relative to the median grain size of the bed are based on flume data from a relatively constrained set of experimental conditions. While their qualitative conclusions are plausible, the quantitative applicability of their data to natural settings is uncertain. The bed surfaces studied had nearly identical sorting, a small range of median grain sizes, and mostly bimodal size distributions, and were composed of only fine gravel and sand. In fact all previous friction angle studies [*Miller and Byrne*, 1966; *Li and Komar*, 1986; *Kirchner et al.*, 1990] used experimental man-made or flume-made surfaces with controls and constraints on parameters such as grain size, shape, rounding, packing, and sorting. These limitations, as well as a lack of field comparisons of the friction angle data obtained from experimental surfaces, motivated our efforts to document friction angle properties of natural streambed surfaces with a wide variety of grain sizes and no investigator-imposed constraints. Application of such data to *Wiberg and Smith*'s [1987] critical shear stress model as modified by *Kirchner et al.* [1990] should provide insights into grain mobility and transport on natural surfaces.

Here we present the first friction angle data from naturally formed gravel surfaces of a streambed. These data reveal a dependency of friction angle on degree of surface sorting. In addition, the probability distributions of friction angle and critical boundary shear stress were found to vary greatly with grain size for a given bed surface. Critical shear stress distributions for various grain sizes on a given surface show a common minimum value, but predict that beyond this

[1]Now at the Department of Geological Sciences, University of Washington, Seattle.

Paper number 91WR02529.
0043-1397/92/91WR-02529$05.00

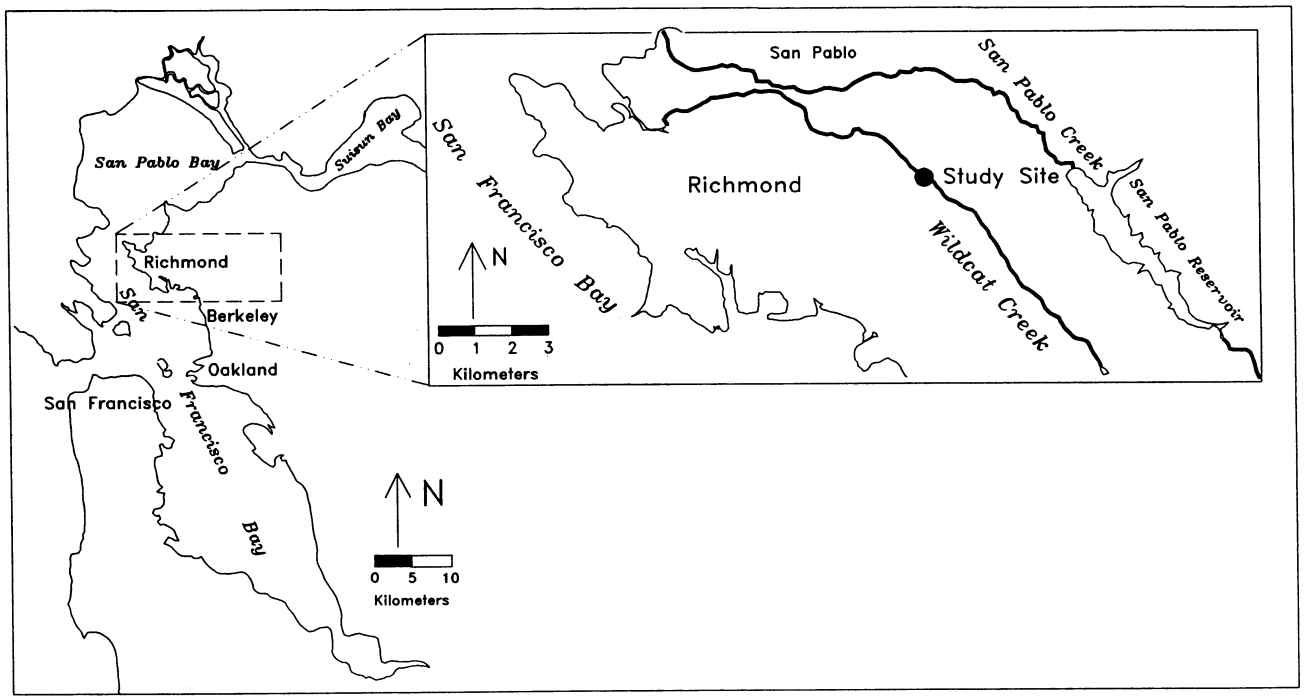

Fig. 1. Study site location map within the bay area of northern California.

origin the larger the mobile grain relative to the bed surface, the smaller the range and value of critical shear stress (indicating a greater ease of mobility for large grains relative to small ones). Our results add further support to the three hypotheses listed above, but disagree with some transport studies using tracer grains. Although grain transport studies are divided and conflicting with regard to relative grain mobility, our results appear inconsistent with those studies which demonstrate a tendency for small grains to have a higher relative percentage of entrainment [e.g., *Andrews and Erman*, 1986; *Ashworth and Ferguson*, 1989; *Kuhnle and Southard*, 1988]. We suggest that other factors, not readily included in friction angle measurements or theoretical calculations, must be considered in order to understand the observed relative mobility of grains.

Study Site and Methods

Wildcat Creek, a gravel-bedded stream immediately north of Berkeley, California (Figure 1) was selected for sampling for a variety of reasons. As part of a stream rehabilitation project, detailed topographic surveys and surface sediment size maps have been made (L. Collins, manuscript in preparation) (Figure 2). Three years of painted rock studies document movement of different sizes of sediment over the various mapped bed surfaces (W. E. Dietrich and L. Collins, manuscript in preparation). The channel becomes entirely dry by the end of summer, enabling sampling of the surface. Excellent access to the channel permitted removal of often heavy surface samples without disturbance.

The creek lies in a narrow valley without a floodplain and is bounded on one side by a relatively steep slope which is shedding large quantities of unsorted debris via earthflows that often extend from the drainage divide to the channel. Despite confinement and the large influx of sediment, the channel meanders and has a well-defined channel geometry. Except for the coarser patches of the bed, the bed surface along much of the creek lacks a coarse surface layer and is extremely mobile: At discharges less than 5% bank-full discharge significant grain displacement occurs on some bars (W. E. Dietrich and L. Collins, manuscript in preparation). The grains are rounded and composed of varying lithologies, including basalt, sandstone, and chert. At the collection sites indicated in Figure 2, the average gradient of the bed is about 0.01, the bank-full width about 5–12 m, depth about 0.3–0.6 m and bank-full discharge approximately 3.4–5.7 m^3/s.

Undisturbed samples of the bed surface were obtained by applying a thin epoxy resin to areas approximately 0.3–0.4 m by 0.3–0.4 m. Experimentation with mixing ratios yielded a suitably strong, low-viscosity adhesive that did not fill pore spaces or alter grain texture. The hardened rigid surfaces were excavated, brought into our laboratory, bedded in a sand and resin mixture in order to provide underlying strength, and mounted in a wooden frame. Grain geometry and texture were maintained during the collection process. Because the samples are composed of surface grains of the bed, we here refer to the samples as "peels" for simplicity.

The three most common bed surface textures found in the stream were sampled. Two samples of the predominant surface texture (sand, gravel, and cobble size, Figure 2) were collected, as well as one each of the other two most common textures (sand and gravel, and gravel and cobble sizes, Figure 2); the cobble and boulder size range (Figure 2) was less common and the grains were too large to sample. Four different locations were used, but the fracture of one of our peels into two nearly equal areas generated a fifth sample (Figure 2). Samples were chosen within an area of a certain texture by placing a wire frame on the bed while looking away. The frame was placed parallel to flow direction, and sampling of extreme bed topography (bar fronts, etc.) was avoided.

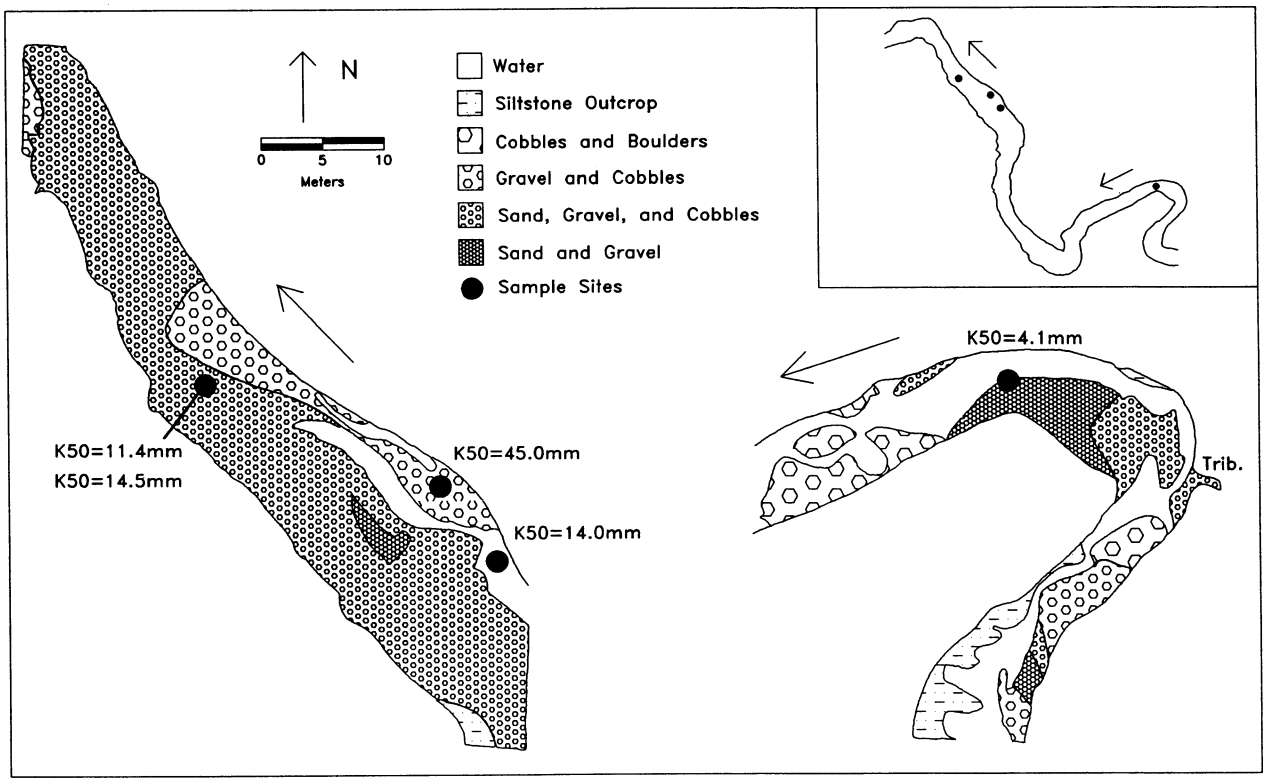

Fig. 2. Study reach of Wildcat Creek, showing sample sites and bed surface grain size variation. Based on map appreciatively borrowed from L. Collins (manuscript in preparation). Original map drawn in 1987 during low flow. Arrows indicate flow direction. Bed textures classified according to L. Collins (manuscript in preparation).

Grain size of each peel was determined by randomly lowering a hand-held needle (while the operator looked away) onto the surface and measuring the selected grain's apparent intermediate axis with a caliper which could be read to 0.01 mm. The precision of these measurements was to the nearest 0.1 mm for grains about 8 mm or less and to the nearest 1 mm for larger grains. The peels were periodically rotated to insure random grain selection. This is a random sampling method popularly accepted as being equivalent to the grid-by-number method used by *Wolman* [1954] and *Leopold* [1970]. *Kellerhals and Bray* [1971] and *Diplas and Sutherland* [1988] have shown that the grid-by-number method produces comparable results to the traditional sieve by weight sampling; however, the comparisons of *Kellerhals and Bray* [1971] are limited to grains greater than 8 mm. Two pebble counts of 75–100 grains each were conducted and combined into a single data set for each peel.

Following *Miller and Byrne*'s [1966] procedure, we measured friction angles by placing selected grain sizes on the peels and tilting the peels in the downstream direction until the grains moved out of their pockets. The angle of tilt of the peel at this point is the friction angle for the grain of interest. A wooden tilting apparatus was constructed that allowed friction angles to be measured from 0° to 110° at 5° intervals. The tilting was accomplished by mounting the peels onto a board hinged at one end and slowly raising and stopping at 5° intervals.

Test grains were randomly placed on the peels by dropping them from a short distance above the surface. The grains were not allowed to touch each other, but otherwise random placement and orientation was attempted. Friction angles were measured by slowly raising the tilt table and recording the grains that moved at the end of each successive 5° inclination. Grain motion was defined as movement of a minimum of one grain diameter via sliding, rolling or both. Test grains that were set in motion by collision with another moving grain were not counted. Friction angle distributions for a given test size on each peel are based on the recorded motion of 100–300 grains (Table 1).

The test grains used to measure friction angles on each peel were natural grains collected from Wildcat Creek. Five ranges of test grain sizes approximating 4–64 mm were used (Table 1). Not all the tests included the 64-mm size, because grains this large tended to damage the surface as they rolled. The 8- to 64-mm test grains were obtained by sieving gravel from the site and selecting grains by hand that had intermediate diameters close to the desired grain size. The 4.5-mm grains simply represent the 4- to 4.8-mm sieve range of the collected gravel. In addition, long and short axes were recorded, and then the grains were painted and numbered so that they could be easily tracked during the tilting tests. Painting did not appear to greatly alter individual grain roughness. The Corey shape factor (CSF, Table 1) [*Blatt et al.*, 1980] ranged from 0.57 to 0.68.

RESULTS

Sediment Size Distribution

Figures 3 and 4 show the grain size distributions and photographs of the five peels. The data for Figure 3 are listed in Table 2. The median grain sizes of the peels (K_{50}, as used

TABLE 1. Test Grain Sets

	4.0–4.8 mm	7.2–9.0 mm	15–18 mm	30–34 mm	62–67 mm
Average b axis, mm	4.5	8.0	16	33	64
Average CSF*	0.68	0.63	0.57	0.57	0.57
n_s (number of grains per set)	172	38	33	19	5
n_p (number of grains used on peel):					
K_{50}† = 4.1 mm	300	200	287	190	
K_{50} = 11.4 mm	299	499	194	189	100
K_{50} = 14.0 mm	300	200	196	190	
K_{50} = 14.5 mm	300	200	194	190	150
K_{50} = 45.0 mm	197	200	193	193	198

Note that average b axis values remained constant even though n_p varied.
*CSF = $d_S/(d_L d_I)^{1/2}$ where d_S, d_L, and d_I are the short, long, and intermediate grain diameters.
†K_{50} is the median surface grain size of a given peel (see Table 2).

by *Kirchner et al.*, [1990]) are 4.1 mm, 11.4 mm, 14.0 mm, 14.5 mm and 45.0 mm. Successive pebble counts of about 100 grains each for the 11.4-mm, 14.0-mm, and 14.5-mm surfaces showed a variation in K_{50} of less than 1 mm. Two pebble counts of 75–100 grains each for the 45.0-mm and 4.1-mm surfaces showed variations in K_{50} of about 5 mm and less than 1 mm respectively. Variation in standard error between successive pebble counts for a given peel was less than 1 mm for all surfaces. Standard error increases with K_{50}. The combined pebble count data for each peel showed that sorting varied, but not with the median grain size as otherwise might be expected. The 4.1-mm peel was best sorted (σ = 0.71, Table 2) and the 14.5-mm peel was most poorly sorted (σ = 1.35). The other three samples had nearly identical sorting of approximately σ = 1.0 (Table 2). As the photographs reveal (Figure 4), the surfaces also appear to differ in packing and the degree of infilling of grain pockets by fines. Clearly the 45.0-mm peel is quite rough. However, note that the 14.5-mm surface appears smoother than the 14.0-mm peel which has nearly the same median grain size, but is better sorted. In other words, the smoother texture of the 14.5-mm peel is presumably due in part to poorer sorting, allowing more grain pockets to be filled in by fines. However, *Kirchner et al.* [1990] point out that packing of grains can vary greatly even with relatively small differences in grain size distribution.

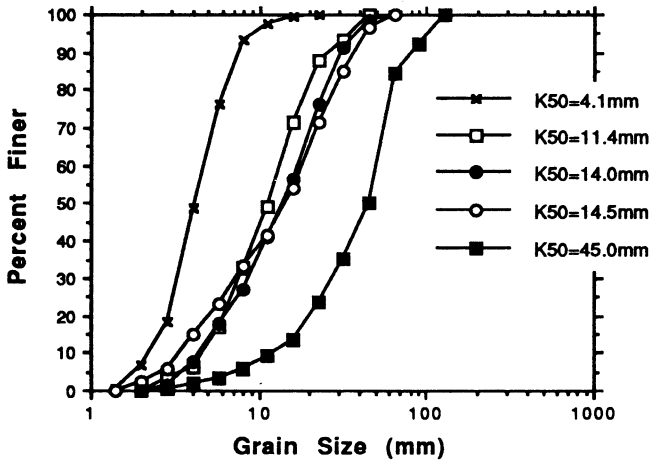

Fig. 3. Cumulative grain size distributions for the five peels. K_{50} is the median bed surface grain size.

Friction Angle Distributions

The results of the tilting tests are listed in Table 3 where they are arranged to show friction angles for the five surfaces as percentiles of the friction angle distributions for the various test grains. The standard deviation for friction angles measured by test grains averaged over all the peels was about 15°. In addition, on one surface five replicate runs of about 100 grains each using different observers showed standard deviations similar to within 3°. On the same surface there was a ±2° variation in Φ_{50} using different observers, correlating well with a standard error of ±2° for each replicate run.

The variability of these surfaces is such that the range of friction angle was from 20° to often greater than 100°, regardless of the size of the test grain relative to that of the surface. Whereas the coarsest grains tended to move mostly at lower friction angles, the smaller grains had a more uniform friction angle distribution (Figure 5). Hence, the cumulative friction angle distributions (Figure 6) systematically steepen with increasing grain size. These differences in friction angles lead to important variations in critical boundary shear stress, as we will discuss later.

Miller and Byrne [1966] proposed an empirical relationship similar to

$$\Phi_{50} = \alpha(D/K_{50})^{-\beta} \quad (1)$$

to define the dependence of the median friction angle, Φ_{50}, on the ratio of the grain size of interest, D, to the median grain size of the surface, K_{50}. Although this equation fits previous researchers' friction angle data well, *Kirchner et al.* [1990] noted that it cannot be strictly correct, because as a nonspherical test grain becomes very large relative to the bed surface grain size, the friction angle approaches a finite value (roughly 20°–30°) controlled by grain shape, rather than declining to zero. *Miller and Byrne* [1966] proposed that the coefficient α is a function of grain shape and roundness, while the exponent β varies with sorting. *Li and Komar* [1986] have also shown that α is dependent on grain shape and roundness, as well as packing. As *Kirchner et al.* [1990] point out, there is no correlation of absolute values for β or α with grain shape and sorting across studies. This may be in part due to the inability to accurately quantify packing variations and their effects on friction angles.

Equation (1) is fitted separately to data from each of the five peels (Figure 7), revealing important differences between naturally formed surfaces and ones formed artificially

Fig. 4*a*. K_{50} = 4.1 mm

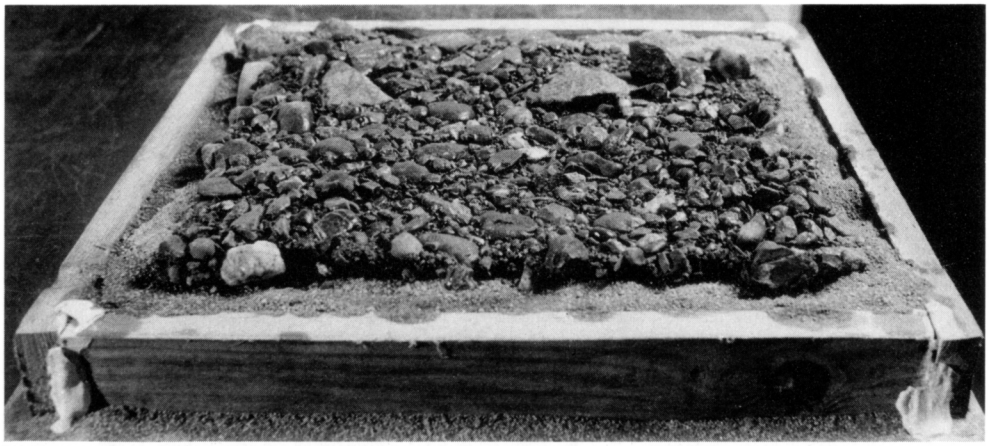

Fig. 4*b*. K_{50} = 11.4 mm

Fig. 4*c*. K_{50} = 14.0 mm

Fig. 4. The peels used to determine friction angles for the three most common grain size ranges found in Wildcat Creek. K_{50} is the median grain size for each sample. Widths of the wooden frames for Figures 4*a*–4*e* are 43 cm, 41 cm, 51 cm, 39 cm, and 45 cm, respectively. Flow direction is toward the camera in all cases. Note that although the 11.4-mm, 14.0-mm, and 14.5-mm surfaces have similar K_{50} values there are distinct differences in surface texture due to the effects of sorting and packing variations. Both the 11.4-mm and 14.5-mm peels have a smoother appearance than the 14.0-mm surface.

Fig. 4*d*. K_{50} = 14.5 mm

Fig. 4*e*. K_{50} = 45.0 mm

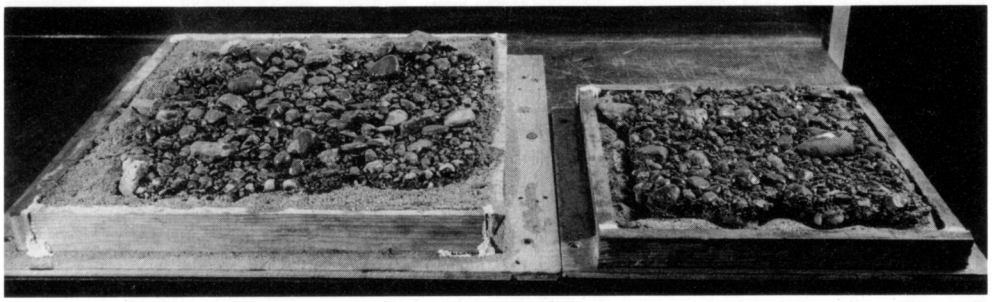

Fig. 4*f*. Comparison of 14.0-mm and 14.5-mm peels

Fig. 4. (continued)

in previous studies. As shown in Figure 8, the coefficient α correlates with surface sorting of the peels. The exponent β, however, only weakly correlates (r^2 of 0.32) with the sorting parameter σ. Interestingly, these results are directly contrary to the dependencies of α and β as proposed by *Miller and Byrne* [1966]. The exponent β is also in general lower than previously reported values (see Table 4 of *Kirchner et al.* [1990] for summary of data). The correlation of α with sorting could not be examined in the flume data of *Kirchner et al.* [1990], because the sorting (as defined in the notes for Table 2) was nearly the same for all water-worked surfaces in their study (σ = 0.8–1.1). While our data show a strong

TABLE 2. Peel Grain Size Distributions

Grain size, mm	Cumulative Percent Finer				
	K_{50} = 4.1 mm	K_{50} = 11.4 mm	K_{50} = 14.0 mm	K_{50} = 14.5 mm	K_{50} = 45.0 mm
1.4	0.6	0.0	0.0	0.0	0.0
2.0	6.8	0.0	0.0	2.4	0.0
2.8	18.2	3.5	1.5	5.7	0.7
4.0	48.9	6.5	7.5	15.2	2.0
5.7	76.1	17.0	17.9	23.2	3.3
8.0	93.2	33.0	26.9	33.2	5.9
11.3	97.7	49.5	41.3	41.7	9.1
16.0	99.4	71.5	56.7	54.0	13.7
22.6	100.0	88.0	76.1	71.6	23.5
32.0		93.0	91.5	84.8	35.3
45.3		100.0	98.5	96.7	50.3
64.0			100.0	100.0	84.3
90.5					92.2
128.0					100.0
	K_{50} = 4.1 mm	K_{50} = 11.4 mm	K_{50} = 14.0 mm	K_{50} = 14.5 mm	K_{50} = 45.0 mm
n*	176	200	201	211	153
σ†	0.71	0.99	1.14	1.35	1.05
SE‡	0.2	0.8	0.9	1.1	2.6

*Here, n is the number of grains sampled.

†Here, σ is the sorting parameter, calculated as $\sigma = 3.32\ (\log K_{84} - \log K_{16})/4 + 3.32\ (\log K_{95} - \log K_5)/6.6$ [*Blatt et al.*, 1980], where the logarithmic transformation of the grain size is done to normalize the data in order that conventional moment analysis, such as the sorting parameter, can be applied.

‡SE is the standard error in millimeters for the calculated average grain size.

correlation between α and sorting, it should be cautioned that we have not conducted an exhaustive study on the subject; further investigation focused on sorting effects would be valuable.

Poor sorting may tend to reduce the median friction angle by causing deep pockets on the surface to be less common and shallow ones to be more common (Figure 9). Comparison of the 14.5-mm and the 14.0-mm surfaces illustrates this concept. The two surfaces have essentially the same K_{50}, but the 14.5-mm surface is more poorly sorted (Figure 8), producing a smoother surface (Figure 4) and lower Φ_{50} (Figure 7 and Table 3) due to infilling of grain pockets by fines. However, packing is another surface property that is somewhat independent of sorting and may also strongly influence friction angle distributions. For nearly the same surface grain size distribution, the tops of larger grains may protrude well above the mean bed surface or they may lie nearly at the mean bed level. This can be understood by looking at the photographs in Figure 4 and imagining walking on the surfaces such that the larger grains are selectively pushed down, giving the bed a much smoother appearance and reducing both the variance and magnitude of the friction angle. This packing of grains may contribute to a spurious correlation between sorting and the parameters in (1), but we have not developed a method of quantifying bed packing in order to investigate this effect.

Discounting the 45.0-mm peel, there is a good correlation ($r^2 = 0.89$) between K_{50} and σ, the sorting parameter. Assuming this is a valid correlation, spurious variance is introduced in (1) by conflating the effects of D/K_{50} with σ. Thus, we have modified (1) to include σ as a separate variable,

$$\Phi_{50} = \alpha(D/K_{50})^{-\beta}\sigma^{-\gamma} \tag{2}$$

Other relationships to express σ as a variable of Φ could be developed, but we prefer to expand on *Miller and Byrne*'s [1966] simple empirical equation.

To define the site's general variation of α, β, and γ with friction angles other than the median values, we have combined the data for all the peels into a single set. The full range of friction angles, rather than just the median, can be expressed by extending (2) to read

$$\Phi_n = \alpha_n(D/K_{50})^{-\beta_n}\sigma^{-\gamma_n} \tag{3}$$

where Φ_n is the nth percentile friction angle, and α_n, β_n, and γ_n are fitted individually through a simple multiple regression of D/K_{50} and σ for each value of n (Table 4). Both D/K_{50} and σ are statistically significant (with a 95% confidence level for both t and F statistics); however, D/K_{50} is the dominant variable controlling Φ. Regression of α, β, and γ values for n equal to 10–80 yields

$$\alpha_n = 25 + 0.57n \tag{4}$$

$$\beta_n = 0.16 + 0.0016n \tag{5}$$

$$\gamma_n = 0.21 + 0.0027n \tag{6}$$

with r^2 of 0.99, 0.91, and 0.89 respectively. Combining (3), (4), (5), and (6) produces a general expression for friction angle variation in the combined data of our five surfaces:

$$\Phi_n = (25 + 0.57n)(D/K_{50})^{-(0.16 + 0.0016n)}(\sigma)^{-(0.21 + 0.0027n)} \tag{7}$$

In order to determine the accuracy of (7), predicted values for each peel were compared with the observed study values (Figure 10). Except for a few cases there is reasonably good agreement between predicted and observed values. Discrep-

TABLE 3. Friction Angle Distributions by Test Grain for Each Peel

	Test Grain Size				
	4.5 mm	8 mm	16 mm	33 mm	64 mm
			K_{50} = 4.1 mm		
Φ_{10}	33	31	25	22	
Φ_{20}	42	37	29	27	
Φ_{30}	49	42	33	31	
Φ_{40}	56	46	37	34	
Φ_{50}	60	51	41	36	
Φ_{60}	67	56	45	39	
Φ_{70}	75	61	50	44	
Φ_{80}	83	67	56	49	
Φ_{90}	104	74	64	54	
Φ_{100}	>110	>110	>110	85	
			K_{50} = 11.4 mm		
Φ_{10}	39	32	27	25	23
Φ_{20}	47	38	32	29	26
Φ_{30}	53	44	36	32	27
Φ_{40}	59	49	41	34	29
Φ_{50}	68	55	46	39	31
Φ_{60}	77	59	50	43	34
Φ_{70}	87	66	54	47	38
Φ_{80}	101	73	60	51	43
Φ_{90}	>110	80	71	57	49
Φ_{100}	>110	>110	95	95	80
			K_{50} = 14.0 mm		
Φ_{10}	35	32	30	27	
Φ_{20}	47	39	38	33	
Φ_{30}	55	47	47	37	
Φ_{40}	65	52	51	41	
Φ_{50}	71	56	55	45	
Φ_{60}	79	64	60	49	
Φ_{70}	89	72	66	53	
Φ_{80}	108	80	73	58	
Φ_{90}	>110	95	85	67	
Φ_{100}	>110	>110	>110	90	
			K_{50} = 14.5 mm		
Φ_{10}	34	30	25	24	25
Φ_{20}	45	37	31	28	28
Φ_{30}	50	42	34	32	30
Φ_{40}	56	48	36	35	33
Φ_{50}	61	53	40	38	35
Φ_{60}	68	58	45	42	38
Φ_{70}	78	64	49	45	41
Φ_{80}	93	69	55	51	45
Φ_{90}	>110	78	65	57	52
Φ_{100}	>110	>110	>110	85	75
			K_{50} = 45.0 mm		
Φ_{10}	44	35	39	35	27
Φ_{20}	52	44	49	43	35
Φ_{30}	66	56	57	48	40
Φ_{40}	82	66	65	52	45
Φ_{50}	97	71	71	55	49
Φ_{60}	>110	79	77	61	52
Φ_{70}	>110	91	84	69	55
Φ_{80}	>110	108	91	77	60
Φ_{90}	>110	>110	109	90	68
Φ_{100}	>110	>110	>110	>110	>110

Data represent friction angle values in degrees.

ancies may reflect the effects of combining all of the peels into one data set for (7). This combined equation differs from that found to represent the flume-made surfaces studied by *Kirchner et al.* [1990]; they found that with a relatively constant sorting of 0.8–1.1,

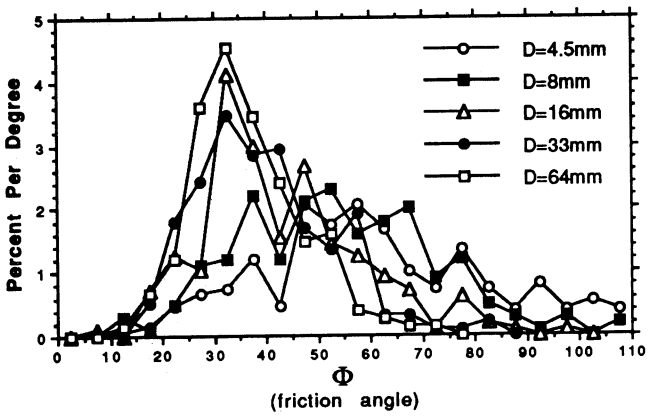

Fig. 5. Friction angle distributions (as a probability density function) for test grains on the 14.5-mm peel. The larger grains predominantly move for a small range of low friction angles, while the smaller grains have a fairly uniform distribution across the full range of friction angles.

$$\Phi_n = (30 + 0.5n)(D/K_{50})^{-0.3} \tag{8}$$

Hence while the function for α is quite similar, there is a large and systematic variation in β for our surfaces that is not observed in the *Kirchner et al.* [1990] experiments. The cause of this difference is unknown.

For a given D/K_{50}, the variation in friction angle with percentile considered is much greater than the variation in median friction angles between surfaces. For the case of D/K_{50} and σ both equal to 1, (7) predicts that the friction angle varies from 31° to 71° between the 10th and 80th percentiles. In contrast, the median friction angle between surfaces varied from 46° to 60° (Figure 7). For grains entrained by drag forces, critical boundary shear stress is proportional to the tangent of the friction angle [e.g., *Wiberg and Smith*, 1987; *Komar and Li*, 1986]; hence critical stress would vary by slightly less than fivefold between the 10th and 80th percentiles of an individual surface, but the median would vary only by about twofold between the different surfaces. As mentioned above, the between-peel variance can be correlated to sorting.

Critical Boundary Shear Stress

Critical boundary shear stress distributions for test grains placed on the peels (Figure 11) were calculated from the *Wiberg and Smith* [1987] theory as modified by *Kirchner et al.* [1990]. Critical shear stress is expressed as a function of grain protrusion and friction angle as follows:

$$\tau_{cr} = (\rho_s - \rho) g \pi \frac{D^3}{6} \left(\frac{1}{\tan \Phi} \frac{C_D}{2\kappa^2} \cdot \int_{p-e}^{p} \{D^2 - [2z - (2p - D)]^2\}^{1/2} f(z)^2 \, dz + \frac{\pi}{8} \frac{C_L}{\kappa^2} D^2 [f(p)^2 - f(p - D)^2] \right)^{-1} \tag{9}$$

where

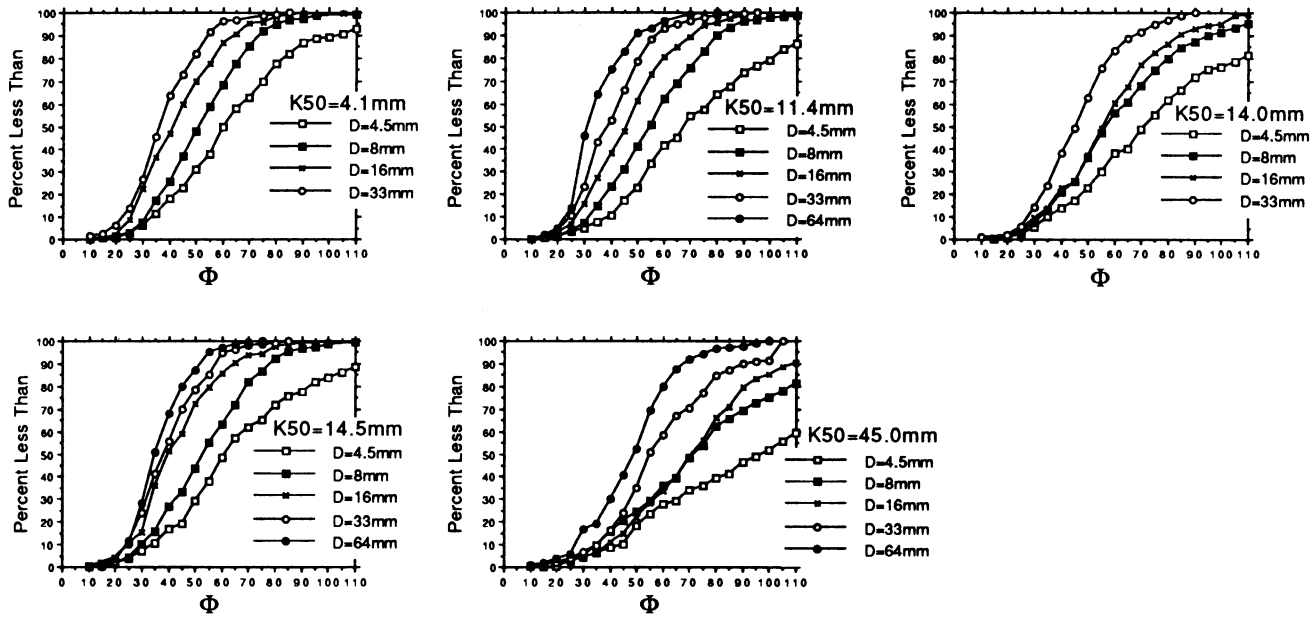

Fig. 6. Cumulative friction angle distributions for test grains placed on each peel. Note the narrow range of friction angles for large grains and the broad spread for small grains. There is also a general divergence of the distributions from a common minimum value.

$$f(z) = \ln\left(\frac{z + z_0}{z_0}\right) \qquad z \geq 0$$

$$f(z) = 0 \qquad z \leq 0$$

and where τ_{cr} is the critical boundary shear stress, g is the gravitational acceleration, ρ_s and ρ are the grain and fluid densities respectively (2.65 g cm^{-3} and 1 g cm^{-3}), D is the grain diameter, Φ is the friction angle, C_D is the drag coefficient (set equal to 0.4), C_L is the lift coefficient (set equal to 0.2), κ is von Karman's constant (equal to 0.407), and z is the height above the bed (see *Kirchner et al.* [1990] for derivation).

The grain protrusion above the bed is composed of two parts, projection, p, which is the level of the top of the grain with respect to the vertical velocity profile, and exposure, e, which is the fraction of the grain not shielded by nearby upstream grains and therefore affected by the flow. We used the empirical results of *Kirchner et al.* [1990] which showed that distributions of protrusion and exposure can be calculated from observed friction angle distributions, but that protrusion, exposure and friction angle were not correlated with each other for individual grains. *Kirchner et al.* [1990] showed that, on their surfaces, the nth percentiles of the projection and exposure distributions of a given grain size could be calculated from the friction angle distribution as

$$e_n = 1/2(D - K_{50} + (D + K_{50}) \cos \Phi_{100-n}) \qquad (10)$$

$$p_n = e_n + K_{50}\pi/12$$

However, as *Kirchner et al.* [1990] point out, it should be cautioned that (10) is derived from the limited fabrics and textures of their flume-made surfaces and may not be valid for other surfaces.

Because of the apparent statistical independence of protrusion, exposure, and friction angle [*Kirchner et al.*, 1990],

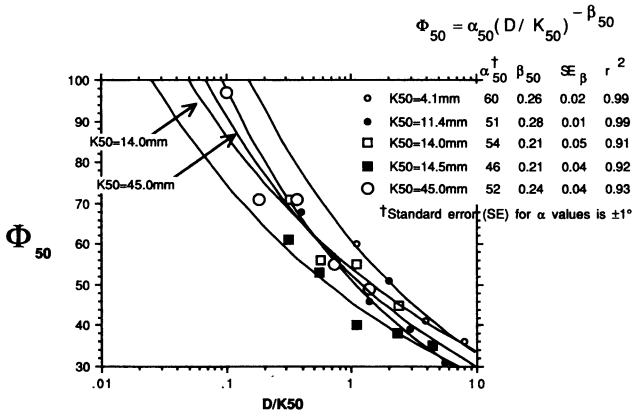

Fig. 7. Median friction angle, Φ_{50}, as a function of grain size, D, relative to the median surface size, K_{50}, for each of the peels. Curves fit using *Miller and Byrne*'s [1966] power function. Note the rapid increase in friction angle with decreasing D/K_{50}.

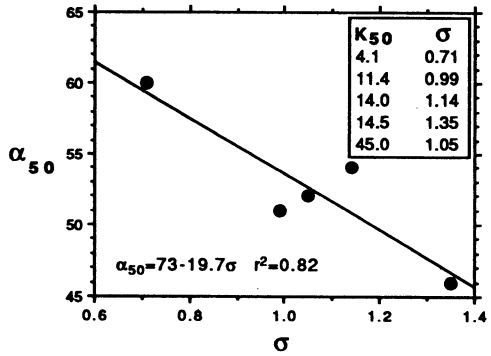

Fig. 8. Correlation of sorting, σ, and α_{50} for the five samples. Sorting parameters calculated according to the method presented by *Blatt et al.* [1980] (see notes for Table 2).

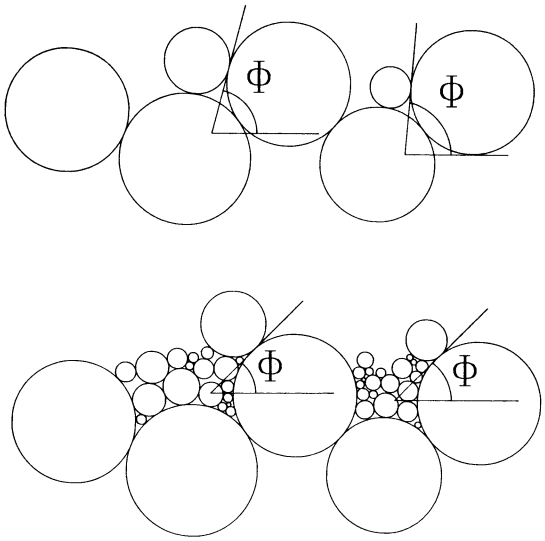

Fig. 9. Diagram showing the reduction of friction angles due to infilling of pockets by fines with decreased (poorer) sorting.

TABLE 4. Multiple Regressions of Percentiles of the Friction Angle Distributions; All Peels Combined
$(\Phi_n = \alpha_n(D/K_{50})^{-\beta_n}\sigma^{-\gamma_n})$

n	α*	β	SE_β	γ	SE_γ	r^2
10	30	0.16	0.01	0.23	0.07	0.88
20	37	0.18	0.01	0.24	0.08	0.89
30	43	0.22	0.01	0.31	0.08	0.92
40	48	0.24	0.02	0.36	0.08	0.93
50	52	0.25	0.01	0.38	0.07	0.94
60	58	0.25	0.02	0.37	0.07	0.94
70	65	0.26	0.01	0.41	0.07	0.94
80	72	0.28	0.02	0.41	0.08	0.94

Degrees of freedom are 22 and 21 respectively for n = 10–50 and n = 60–80.
*Standard error (SE) for all α values is ±1°.

we calculated the cumulative probability of a combination of these factors by multiplying each percentile. For example, the 10th percentile Φ, 90th percentile projection, and the 90th percentile exposure combination yields a probability of 0.1 × 0.1 × 0.1 = 1/1000. This is why the calculated

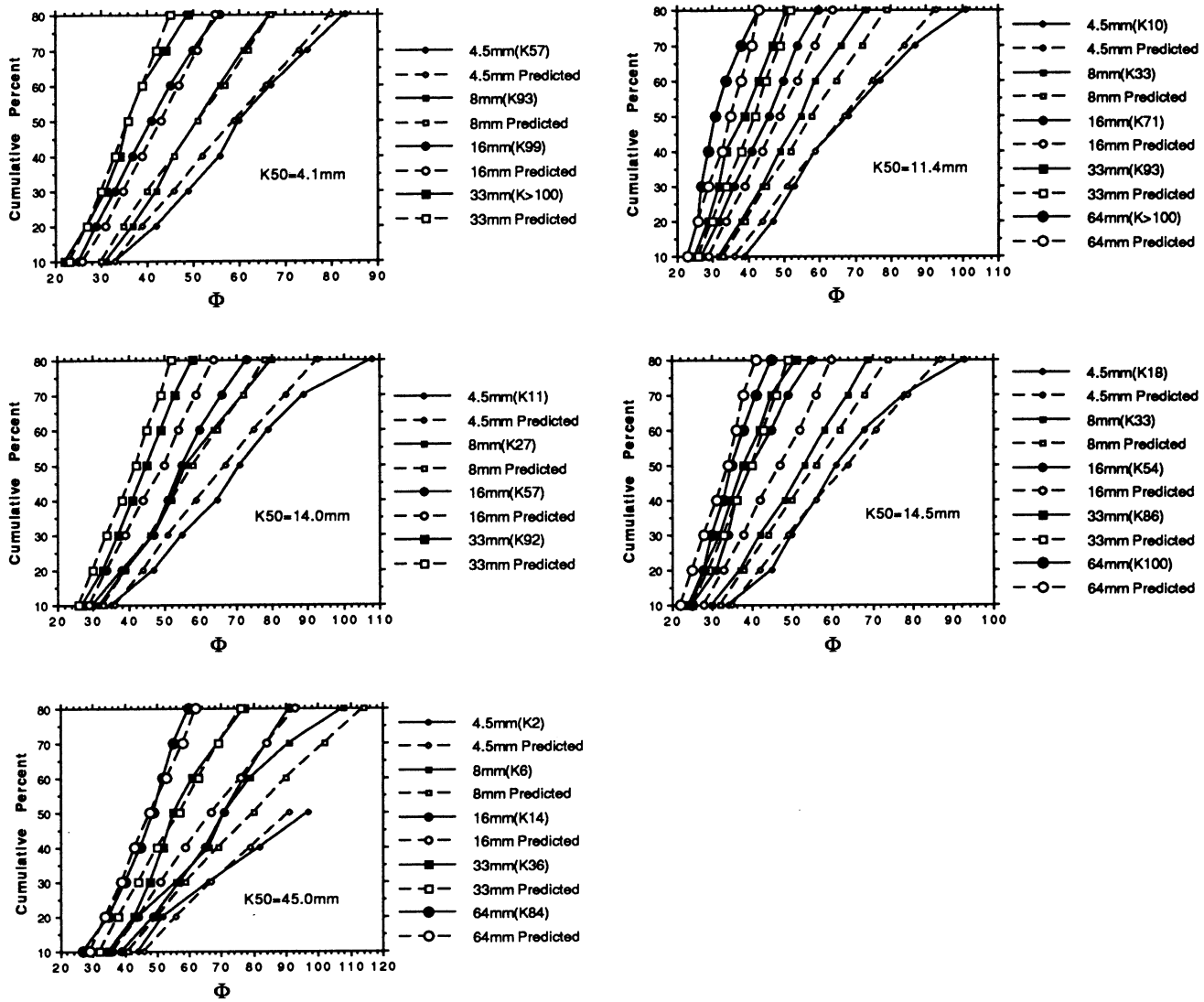

Fig. 10. Comparison of observed (Table 3) and predicted (equation (7)) friction angles for each peel. K values are the percentile of the surface grain size distribution represented by each test grain.

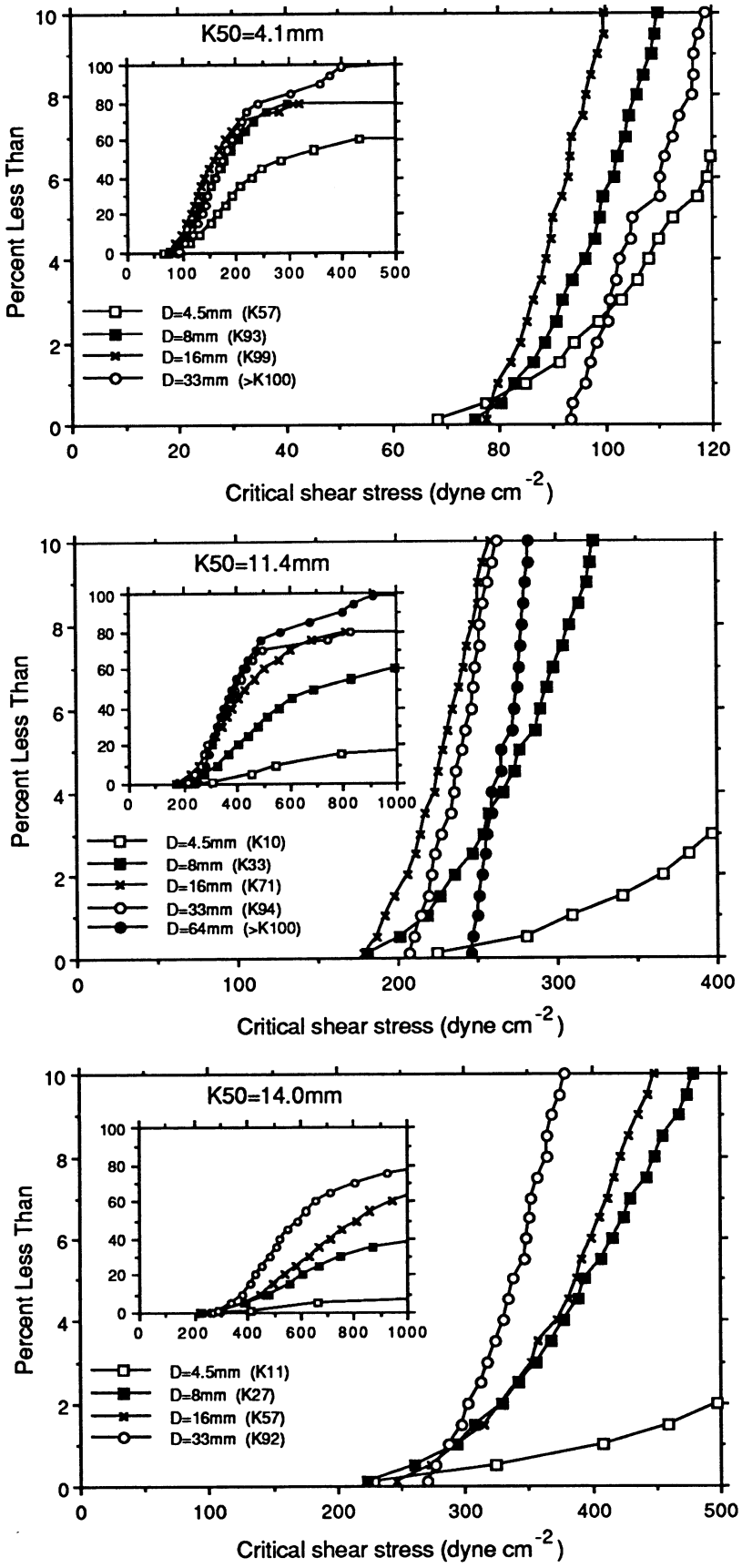

Fig. 11. Cumulative critical shear stress distributions for test grains on each of the peels calculated from the critical shear stress derivation of *Kirchner et al.* [1990] (see text). *K* values are the percentile of the surface grain size distribution represented by each test grain.

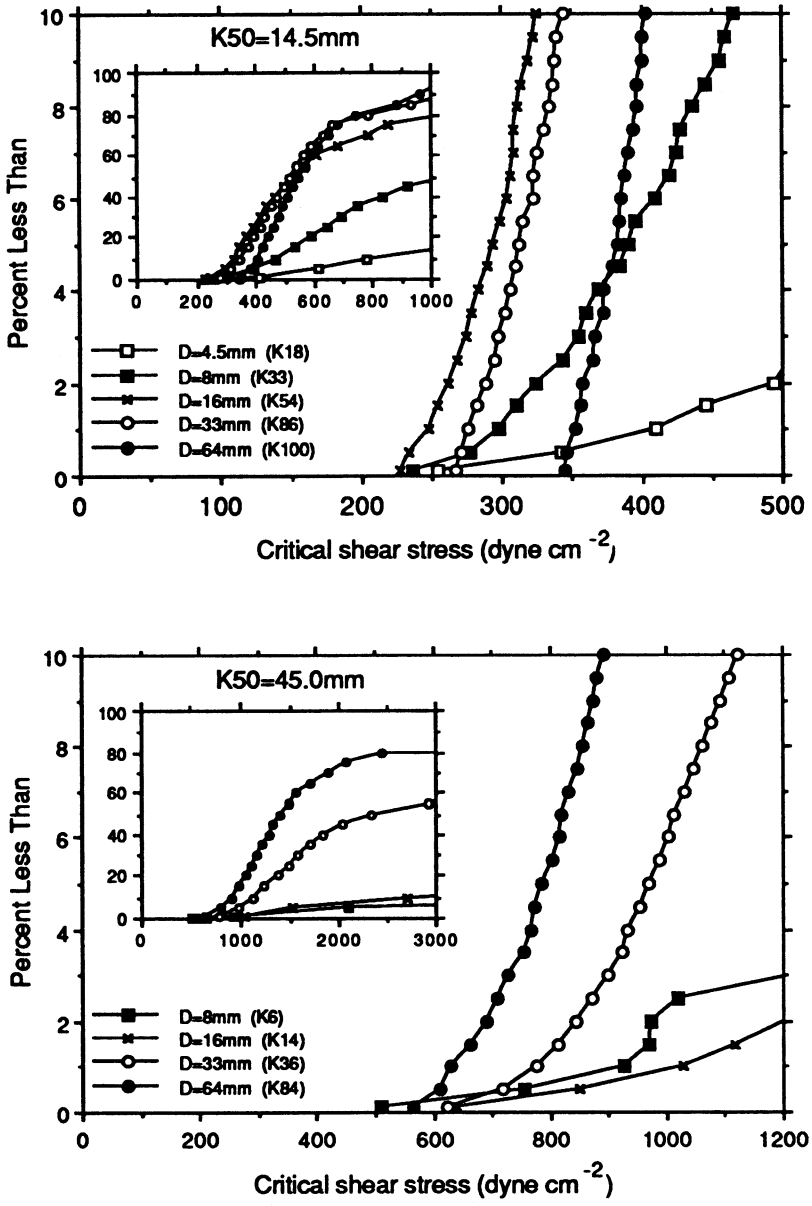

Fig. 11. (continued)

cumulative distributions of critical shear stresses (Figure 11) go nearly to zero.

Kirchner et al. [1990] expressed (9) in a dimensionless form:

$$\tau^*_{cr} = \left(\frac{1}{\tan \Phi} \frac{3C_D}{\pi \kappa^2} \int_{p^* - e^*}^{p^*} [1 - (2z^* - \cdot(2p^* - 1))^2]^{1/2} [\ln (z^* D^* + 1)]^2 \, dz^* + \frac{3C_L}{4\kappa^2} \cdot \{[\ln (p^* D^* + 1)]^2 - [\ln (p^* D^* - D^* + 1)]^2\} \right)^{-1} \quad (11)$$

where

$$\tau^*_{cr} = \frac{\tau_{cr}}{(\rho_s - \rho) g D}$$

$$D^* = \frac{D}{z_0} \approx \frac{10D}{K_{84}} \qquad z^* = \frac{z}{D}$$

$$p^* = \frac{p}{D} \qquad e^* = \frac{e}{D}$$

such that τ^*_{cr} is the dimensionless critical shear stress, z_0 is the roughness term in the law of the wall equation, and K_{84} is the bed surface grain size for which 84% of the grains are smaller. Using (11), the critical shear stress distributions for each peel (Figure 11) can be normalized for variation in bed and test grain size, and combined as shown in Figure 12.

Critical shear stresses calculated here and in the work by *Kirchner et al.* [1990] differ somewhat from those estimated by *Wiberg and Smith* [1987], for three reasons. First, *Wiberg and Smith* [1987] assumed $p = e$, that is, the full area of the grain above the pocket is exposed to the velocity profile

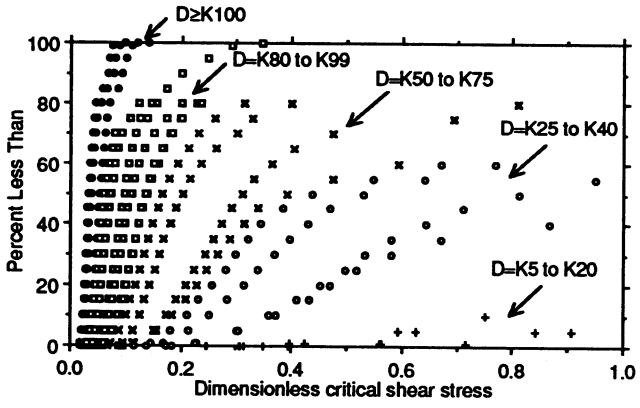

Fig. 12. Cumulative dimensionless critical shear stress distributions for data from all of the peels. Different plot symbols indicate ranges of test grain sizes relative to the median bed grain sizes of the peels.

regardless of what is upstream. While the *Wiberg and Smith* [1987] assumption is useful in defining the minimum critical shear stress, the *Kirchner et al.* [1990] data and inspection of our photographs make it clear that the upstream "hiding" effects can be significant. Second, because we are examining only large roughness Reynolds number flows, we have not included the lift and drag effects of the viscous sublayer. Third, *Wiberg and Smith* [1987] define $z_0 = k_s/30$ (where, in practice, k_s is the median grain size of the bed), whereas we define $z_0 = K_{84}/10$ based on extensive experimental evidence [*Whiting and Dietrich*, 1990] and recent theoretical work [*Wiberg and Smith*, 1991]. When comparable friction angle, protrusion, and z_0 values are used in the original *Wiberg and Smith* [1987] theory and equations (9) and (11), the results are essentially the same [*Kirchner et al.*, 1990].

Four important properties of the critical boundary shear stress distributions of gravel-bedded rivers are suggested by the results shown in Figures 11 and 12. First, on average for a broad range of grain size relative to the median size of the bed surface ($D/K_{50} = 0.1$–8) the calculated minimum critical boundary shear stress (0.1 percentile of the cumulative shear stress distribution) is approximately the same for a given bed surface (Figure 11). Because the parameters of friction angle, projection and exposure are independent stochastic variables, however, any definition of an absolute minimum shear stress value is somewhat arbitrary.

Second, probability distributions of critical shear stress strongly diverge from a common origin, with relatively large particles having a low narrow range of mobilizing shear stress and small grains having a very broad range. A significant fraction of small grains is essentially immobile, trapped within the bed. This result is consistent with *Laronne and Carson*'s [1976] observations; when they placed marked grains on a gravel streambed, they noted (p. 76) that "most of the smaller introduced particles immediately disappeared between and underneath cobbles and boulders." As a result of such selective burial, only a few percent of the small marked particles ($D \approx K_5$) were ultimately recovered, while over 95% of the large ($D \approx K_{50}$) particles were recovered.

Third, minimum critical shear stress varies relatively little across different test grain sizes on an individual bed surface. When these data are plotted as a function of relative grain size (Figure 13) it is apparent that for D/K_{50} greater than 0.7 there is some tendency for "equal mobility" [*Parker and Klingeman*, 1982]. For finer sediment, however, there is strong divergence from equal mobility, except for about the lowest 1% of the critical shear stress distribution. This is a result of the selective trapping of smaller sediment by the bed surface, and suggests that movement of the larger grains is essential for mobilization of smaller ones that may reside in deep pockets.

Fourth, calculated minimum τ^*_{cr} values for $D \approx K_{50}$ are typically close to 0.1 while the commonly reported value is closer to 0.045–0.05 [e.g., *Komar*, 1987*a*; *Komar and Li*, 1988]. If the theoretical calculations are reliable to this level of distinction, then this motivates an explanation based on a well-known, but not well-defined, phenomenon. The empirical studies of critical boundary shear stress have used the mean boundary shear stress calculated from average conditions such as the average water surface slope and flow depth in a flume. Boundary shear stress, however, is characterized by a mean and a variance [i.e., *Grass*, 1971], and as *Kirchner et al.* [1990] suggested perhaps at initial motion turbulent sweeps apply local, short-term shear stress extremes, causing visible motion on the bed. This is consistent with what one commonly observes in flume studies and with the field observations by *Drake et al.* [1988]. Hence, realistic theoretical calculations should imply instantaneous threshold values that are greater than the time-averaged critical shear stresses determined experimentally.

Discussion

Our friction angle measurements and critical boundary shear stress calculations suggest both that for a given bed surface the critical shear stress is approximately the same for all sizes on the bed (at the extreme lower tails of the critical shear stress distributions) and that the finer grains have higher critical shear stresses (above those lower tails). The latter result is at variance with many studies of "selective entrainment" (reviewed by *Komar* [1987*b*]) and with tracer experiments at Wildcat Creek itself. W. E. Dietrich and L. Collins (manuscript in preparation) found that although there is some tendency for large and small grains to move during the same discharge event in Wildcat Creek, in many cases the smaller grains were eroded from a painted patch on the streambed while the coarser grains did not move. Some grain transport studies [*Andrews and Erman*, 1986; *Ashworth and*

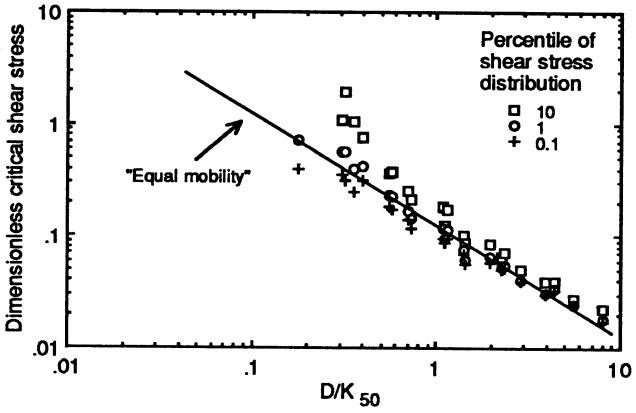

Fig. 13. Dimensionless critical shear stress as a function of test grain size relative to the median surface size. Symbols represent percentiles of the five peels' critical shear stress distributions.

Ferguson, 1989; *Kuhnle and Southard*, 1988] similarly report that for a given event the smaller grains have a higher relative percentage of entrainment.

Critical shear stresses calculated from these friction angle data may not be directly interpretable in terms of stresses required to entrain grains from the bed. Most notably, what have been measured are the friction angles of individual grains placed on the fixed bed, not the friction angles of grains composing the bed surface itself. In this sense, these calculations may be more applicable to "distrainment" (as *Drake et al.* [1988] call grain stopping) than entrainment. In many mixed-grain bed surfaces, including those studied here, the larger grains are often partly buried in the bed, with only a small fraction of the cross-sectional area of the grain exposed to the flow. As the coarse fraction of the bed inevitably tends to be partly buried by the finer fraction, its friction angles should be systematically higher, and their protrusion systematically lower, than our measurements would imply.

Quantifying relative grain burial is difficult. Except when grains are almost completely buried, relative burial has little effect on the exposed plan view grain area; consequently, surface area–based characterizations of gravel size distributions are relatively insensitive to degree of burial.

In these calculations, the relative critical shear stress of different grain sizes is sensitive to how the near-bed flow is characterized. *Kirchner et al.* [1990] assumed that the logarithmic "law of the wall" velocity profile converged to zero at a level defined by the mean bed elevation over a distance of K_{84} on each side of the center of the test grain. They further assumed that the only parts of the test grain exposed to the flow were those protruding above the highest point on the bed surface within a distance of K_{84} upstream of the test grain. In other words, they assumed that each grain on the surface sheds a rectangular wake of length K_{84}. These assumptions are obviously crude approximations, and a more realistic treatment of the complexities of flow around individual grains might yield different conclusions. *Laronne and Carson* [1976], *Brayshaw et al.* [1983], and *Brayshaw* [1985] point out the importance of bed microtopography with regard to relative grain mobility. Differences in shear stress between the stoss and lee sides of a large clast create distinctive textures through selective entrainment and distrainment with stage variations. Flow deflection around large grains should also raise the local shear stresses felt by small grains alongside them.

Despite the uncertainty about these effects on the critical boundary shear stress, it is clearly best characterized as having a probability distribution rather than a single value for any particular D/K_{50}. Consequently, the hypotheses listed above that were proposed by *Kirchner et al.* [1990] based on this experimental result for their flume data are also supported with these data. Specifically, the outwardly high minimum critical shear stress calculated here may be correct in magnitude if grains are primarily entrained by local, transient excursions of high stress associated with sweep events. The apparent greater mobility of well-exposed larger grains should strongly influence the movement of the essentially immobile finer grains. Finally, the probability distributions suggest that with increasing boundary shear stress above some minimum value increasing numbers of grains in more stable resting positions will be moved. Hence, it may be the frequency distribution of friction angles and protrusion that leads to the characteristic steep rise in bed load transport rate with increasing boundary shear stress.

CONCLUSIONS

Our friction angle data, the first obtained from a streambed surface, raise several points about mechanistic studies of initial transport. These data demonstrate the need to obtain such parameters from natural bed surfaces, rather than ones artificially made for testing purposes. Natural surfaces differ in their friction angle properties, and although the *Miller and Byrne* [1966] relationship expressing friction angle as a power function of D/K_{50} can accurately represent the data, the coefficient and exponent of this empirical expression are not universal constants and do not seem to vary in the manner expected by *Miller and Byrne* [1966]. In particular, here we found that the coefficient α varies with sorting, while the exponent β does not. Modification of the *Miller and Byrne* [1966] relationship to include sorting as a separate variable best represents the data. Comparison of naturally worked and flume-made surfaces shows slightly lower α values and systematically lower and widely variable β values for the combined natural surfaces.

In order to use these experimental results in a physics-based model for predicting critical boundary shear stress, bed load transport and sorting, it now seems necessary to expand the *Wiberg and Smith* [1987] type model to include the effects of packing, partial burial and local grain protrusion-induced flow accelerations. Because of these effects, field-based studies that attempt to define friction angle and protrusion should probably be done, if possible, on grains already resting on the bed, rather than on grains placed on the bed. To test a critical shear stress theory it may be most instructive to obtain high-speed motion pictures of a mobile bed in order to document the role of local high shear stresses induced by turbulent sweeps. A challenge yet remaining is to develop theories that can predict particle geometric relationships in order to include the effects described here on critical boundary shear stress.

Acknowledgments. We thank Bob Idelweiller, Judy Journeay, Kevin Schmidt, and Nicol Uhlig for their help in data collection and Nick Cedar for the photographs. This study was funded in part by Project W-734 of the University of California Water Resource Center granted to W.E.D.

REFERENCES

Andrews, E. D., and D. C. Erman, Persistence in the size distribution of surficial bed material during an extreme snowmelt flood, *Water Resour. Res.*, *22*, 191–197, 1986.

Ashworth, P. J., and R. I. Ferguson, Size-selective entrainment of bed load in gravel bed streams, *Water Resour. Res.*, *25*, 627–634, 1989.

Blatt, H., G. Middleton, and R. Murray, *Origin of Sedimentary Rocks*, pp. 48–79, Prentice-Hall, Englewood Cliffs, N. J., 1980.

Brayshaw, A. C., Bed microtopography and entrainment thresholds in gravel-bed rivers, *Geol. Soc. Am. Bull.*, *96*, 218–223, 1985.

Brayshaw, A. C., L. E. Frostick, and I. Reid, The hydrodynamics of particle clusters and sediment entrainment in coarse alluvial channels, *Sedimentology*, *30*, 137–143, 1983.

Diplas, P., and A. J. Sutherland, Sampling techniques for gravel sized sediments, *J. Hydraul. Eng.*, *114*, 484–501, 1988.

Drake, T. G., R. L. Shreve, W. E. Dietrich, P. J. Whiting, and L. B. Leopold, Bedload transport of fine gravel observed by motion-picture photography, *J. Fluid Mech.*, *192*, 193–217, 1988.

Grass, A. J., Structural features of turbulent flow over smooth and rough boundaries, *J. Fluid Mech.*, *50*, 233–255, 1971.

Kellerhals, R., and D. I. Bray, Sampling procedures for coarse fluvial sediments, *J. Hydraul. Div. Am. Soc. Civ. Eng.*, *97*, 1165–1180, 1971.

Kirchner, J. W., W. E. Dietrich, F. Iseya, and H. Ikeda, The variability of critical shear stress, friction angle, and grain protrusion in water-worked sediments, *Sedimentology*, *37*, 647–672, 1990.

Komar, P. D., Selective grain entrainment by a current from a bed of mixed sizes: A reanalysis, *J. Sediment. Petrol.*, *57*, 203–211, 1987*a*.

Komar, P. D., Selective gravel entrainment and the empirical evaluation of flow competence, *Sedimentology*, *34*, 1165–1176, 1987*b*.

Komar, P. D., and Z. Li, Pivoting analyses of the selective entrainment of sediments by size and shape with application to gravel threshold, *Sedimentology*, *33*, 425–436, 1986.

Komar, P. D., and Z. Li, Applications of grain-pivoting and sliding analyses to selective entrainment of gravel and to flow-competence evaluations, *Sedimentology*, *35*, 681–695, 1988.

Kuhnle, R. A., and J. B. Southard, Bed load transport fluctuations in a gravel bed laboratory channel, *Water Resour. Res.*, *24*, 247–260, 1988.

Laronne, J. B., and M. A. Carson, Interrelationships between bed morphology and bed-material transport for a small, gravel-bed channel, *Sedimentology*, *23*, 67–85, 1976.

Leopold, L. B., An improved method for size distribution of stream bed gravel, *Water Resour. Res.*, *6*, 1357–1366, 1970.

Li, Z., and P. D. Komar, Laboratory measurements of pivoting angles for applications to selective entrainment of gravel in a current, *Sedimentology*, *33*, 413–423, 1986.

Miller, R. L., and R. J. Byrne, The angle of repose for a single grain on a fixed rough bed, *Sedimentology*, *6*, 303–314, 1966.

Parker, G., and P. C. Klingeman, On why gravel bed streams are paved, *Water Resour. Res.*, *18*, 1409–1423, 1982.

Whiting, P. J., and W. E. Dietrich, Boundary shear stress and roughness over mobile alluvial beds, *J. Hydraul. Eng.*, *116*, 1495–1511, 1990.

Wiberg, P. L., and J. D. Smith, Calculations of the critical shear stress for motion of uniform and heterogeneous sediment, *Water Resour. Res.*, *23*, 1471–1480, 1987.

Wiberg, P. L., and J. D. Smith, Velocity distribution and bed roughness in high-gradient streams, *Water Resour. Res.*, *27*, 825–838, 1991.

Wolman, M. G., A method of sampling coarse river-bed material, *Eos Trans. AGU*, *35*, 951–956, 1954.

J. Buffington, Department of Geological Sciences, University of Washington, Seattle, WA 98195.

W. E. Dietrich and J. W. Kirchner, Department of Geology and Geophysics, University of California, Berkeley, CA 94720.

(Received March 8, 1991;
revised September 27, 1991;
accepted October 3, 1991.)